Rotating bending fatigue behaviour and quasi-static tensile properties of Wire Arc Additively Manufactured 308L stainless steel

ce/papers Proceedings in civil engineering

Ernst & Sohn A Wiley Brand

ORIGINAL ARTICLE

eurosteel AMSTERDAM 2023

Ernst & Sohn A Wiley Brand

Rotating bending fatigue behaviour and quasi-static tensile properties of Wire Arc Additively Manufactured 308L stainless steel

Davide Leonetti[1] | Max de Munnik[1] | Luuk Kassing[1] | Danish Khan[1] | Jean-Francois Moulin[2] | Bert Snijder[1]

Correspondence

Dr. Davide Leonetti
Eindhoven University of Technology
Department of the Built Environment
Groene Loper 6
Eindhoven, The Netherlands
Email: d.leonetti@tue.nl

[1] Eindhoven University of Technology, Eindhoven, The Netherlands
[2] MX3D, Amsterdam, The Netherlands

Abstract

Wire Arc Additive Manufacturing (WAAM) is a direct energy deposition method used to manufacture steel components by using an electric arc as a heat source to melt a metal wire and deposit it layer by layer. In this study, monotonic tensile tests, standardized Charpy impact tests, and rotating bending fatigue tests are executed to characterize the mechanical properties of WAAM 308L stainless steel using specimens extracted from additively manufactured plates. In particular, monotonic tensile properties are investigated in three directions: that is 0, 90, and 45 degrees with respect to the plane of deposition, whereas the fatigue strength is quantified for one direction only, i.e. 90 degrees since this is deemed to be the weakest.

The mechanical characterization highlights that WAAM 308L SS shows an anisotropic behaviour, an enhanced strain-rate sensitivity, and an overall reduced yield strength as compared to the base material 308L. The anisotropic material behaviour is explained by the microstructure morphology since the austenite grains form anisotropic columnar zones due to an uneven heat profile during production. During the fatigue tests, the relatively high strain rate sensitivity causes susceptibility to self-heating at relatively low loading frequencies, i.e. below 100Hz.

Keywords

Rotating bending, 308L WAAM stainless steel, mechanical characterization, fatigue

1 Introduction

Additive manufacturing and digital fabrication technologies enable the fabrication of complex geometrical parts, while potentially optimizing material usage. Wire arc additive manufacturing (WAAM) is a Directed Energy Deposition (DED) method that makes use of an electric arc as a heat source to melt the wire feedstock and deposit the metal layer by layer [1].

Characterization and observation of the monotonic tensile and cyclic response of the material resulting from additive manufacturing is a topic of interest for research due to common failure modes observed during engineering. Parts manufactured by WAAM are prone to contain defects such as internal pores, cracks, voids, not-melted regions, or lack of fusion defects [2]. These defects may be expected to enlarge the scatter in fatigue life data and reduce the overall fatigue life as compared to non-additively manufactured components.

However, WAAM AISI 304L stainless steel has enhanced or comparable fatigue performance for the transitional (between low- and high-cycle fatigue) and high-cycle fatigue loading regimes compared to wrought and DED-fabricated materials [2]

Dedicated fatigue experiments on WAAM 308L SS were performed by [2], by applying fully reversed axial loading to characterize the low-cycle fatigue behavior of WAAM 308L SS and to compare it with hot-rolled 308L SS. From these experiments, it was found that extracting specimens from WAAM plates leads to longer fatigue life at higher stress amplitudes, i.e. in the low-cycle fatigue regime, and to shorter fatigue life at lower stress amplitudes, i.e in the high-cycle fatigue regime. For low-cycle fatigue, the crack growth life dominates the major portion of fatigue life whilst, for high-cycle fatigue, the crack initiation life dominates [3, 4]. This means that WAAM potentially induces a higher resistance against fatigue crack growth and less resistance against crack initiation. WAAM 308L SS can be considered substantially defect free since no defects were found in their micro-structural analysis [2]. Also, previously recorded fatigue failures did not show signs of failure initiated by pre-existing defects. Therefore, the differences between the fatigue life of WAAM 308L SS and the base

material are not explained by the potential presence of manufacturing defects.

The difference is likely caused by differences in microstructure caused by the production process. As shown in [2, 5] a typical hierarchical layered structure can be found in WAAM 308L SS. These layers are related to the deposition of the melted wire. Between two deposition layers, $<001>$ textured columnar dendrites are found - contrary to the typical randomly textured equiaxed grains in the other regions of the material - resulting in a lower Young's modulus. The transition between the two-grain types is explained on the basis of the melting of the deposition layer which occurs when a new layer is added on top [6]. The process of portions of grains aligning is caused by the non-uniform heat profile in the material during deposition [7, 8]. The columnar zone is an anisotropic region where the grain structure is elongated in the solidification direction of the steel [9]. This results in the dependency of Young's modulus and other tensile properties on the sampling direction [10]. Besides the difference in grain orientation, also a relatively large dislocation density was found in the columnar region, attributing to a higher yield strength [2].

When WAAM components are loaded diagonally to the printing layers, an increased yield stress and Young's modulus are found compared to other orientations [11-14]. Several possible explanations for the differences are found in the literature. The difference in Young's modulus is often explained by a higher portion of the grains that is deformed in the <110> type direction due to fibering, which results in a significantly higher Young's modulus according to the single crystal elastic moduli regression model [11, 15].

In diagonally loaded specimens also a higher yield and ultimate strength, as well as a higher strain at failure are found compared to loading parallel or perpendicular to the deposition planes. As highlighted in [13] this may be caused by the fact that the grain boundaries limit dislocation and act as barriers in the Hall-Petch strengthening mechanism.

Previous research has investigated the anisotropic behaviour of WAAM specimens for quasi-static loading as well as the low-cycle fatigue behaviour of WAAM 308L stainless steel. Nevertheless, research regarding the high-cycle rotating bending fatigue behaviour of stainless steel 308L is not performed.

This research investigates the monotonic strength and the high-cycle rotating bending fatigue response of Wire Arc Additive Manufacturing (WAAM) 308L stainless steel (SS) for a loading direction perpendicular to the deposition plane deemed to be the weakest.

2 Materials and Methods

In this research, tensile, toughness, and rotating bending fatigue tests are executed. The specimens used are extracted from WAAM 308L SS plates, which are fabricated according to the parameters given in Table 1.

The monotonic tensile tests and the Charpy notched bar impact tests are carried out for three orientations with respect to the deposition layers: 0, 45, and 90 degrees. Instead, the rotating bending fatigue tests are carried out in the 90-degree direction only, see Figure 1.

Table 1 Description of the different types of furnishing

Process Parameter	Detail	Value	Unit
Deposition	Current	110	A
Power	Voltage	21	V
Speed	Welding speed	14	mm/s
	Wire feed rate	3.7	m/min
	Deposition rate	1.37	kg/h
Distance and angle	Layer height	2.32	mm
	Electrode angle	90	degrees
Wire	Grade	ER308LSi	
	Diameter	1.2	mm
Shield gas	Type	98%Ar, 2%CO_2	
	Flow rate	16	l/min

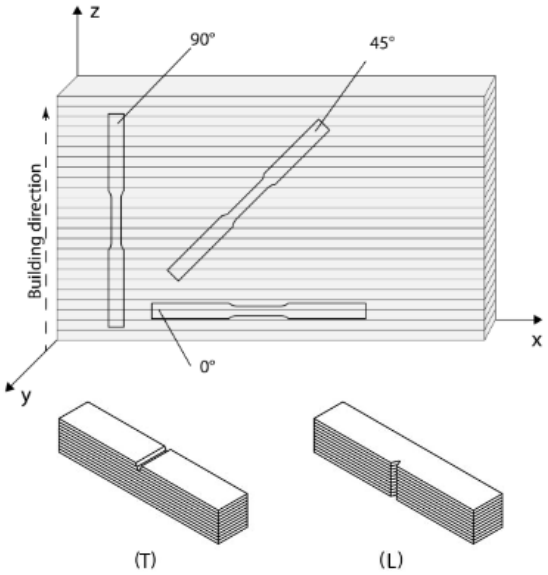

Figure 1 Orientation of the specimens with respect to the deposition layers and different configurations for the Charpy specimens oriented following the 0 degrees orientation.

2.1 Monotonic tensile tests

The monotonic tensile properties of WAAM 308L SS are determined by standardized tensile tests executed on flat plate specimens with rectangular cross-sections according to ASTM E8-21 [16].

The monotonic tensile tests are carried out using an INSTRON 5985 universal testing machine equipped with a 250 kN load cell and by applying a strain rate equal to 0.015 mm/mm/min, in accordance with the aforementioned standard. For one specimen per direction, the strain rate is increased post-yielding to 0.06 mm/mm/min. However, due to a discontinuous material response observed due to the change in the loading speed, it is decided to keep the crosshead speed constant for the other specimens.

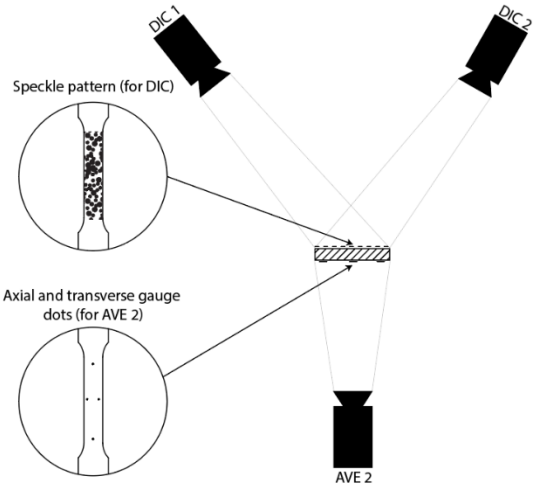

Figure 2 DIC setup for measuring full-field strain and elongation during the tensile test.

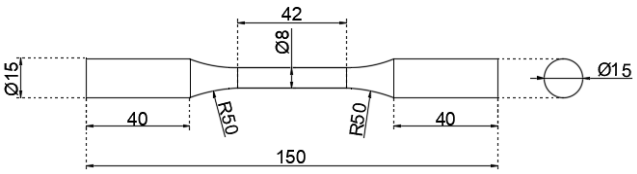

Figure 3 Design of the specimens for the rotating bending tests.

Two separate methods are used to determine the longitudinal and transverse elongation. On one side of the specimen, measurements are performed by using the Instron AVE 2 non-touching video extensometer. On the other side, Digital Image Correlation (DIC) measurements are performed using a stereoscopic DIC setup, Q-400 by Dantec Dynamics, see Figure 2.

For the video extensometer, four dots (gauges) with distances 50 and 8 mm for respectively the axial and transverse direction are placed on one side of the specimen, in compliance with ASTM E8-21 [16]. The sensor data are stored at a sampling rate of 5 samples per second.

During the test, the sampling rate of the DIC system recorder varies. In the elastic range, an image is made at each 1 kN load increase. In the plastic range, a recording is made for every 0.3 mm displacement of the crosshead. From the DIC measurements, both the axial and transverse strain are evaluated. In addition to determining the monotonic tensile properties of the material, DIC also enables the measurement of the full strain field on the surface of the test section. The DIC settings are validated by comparing the axial strain data from DIC to the axial strain data from the extensometer. The settings with the best fit to the extensometer axial strain data are used.

Young's modulus of the material is determined by using Ordinary Least Squares (OLS) regression over the obtained data points of stress versus strain in the linear elastic range of the material as proposed in ASTM E8-21 [16]. The end point of the elastic range is determined by calculating the R^2 metric for each set of points of the stress-strain curve fitted by an OLS linear regression line that goes through the origin and considers all previous points. The point just before the value of the coefficient of determination, R^2, drops significantly below 1.0 indicating the end of the linear elastic range, i.e. the proportionality limit. The Poisson's ratio is determined by plotting the transverse strain against the longitudinal strain, both obtained by DIC, and applying OLS regression over the linear elastic part as determined for calculating the Young's modulus. The 0.2% proof stress and the ultimate stresses and strains, as well as the ultimate engineering stress and strain, are determined according to ASTM E8-21 [16].

Three factors are used to describe the ductility of the material from the monotonic tensile tests. Two are calculated and measured post-failure according to ASTM E8-21, namely the elongation at fracture and the reduction of area. In addition, the modulus of toughness is calculated as the area under the stress-strain curve up to fracture using a trapezoidal integration rule.

2.2 Impact toughness tests

Charpy impact toughness tests are performed in four different directions on standard size Charpy impact specimens according to ASTM E23-18 [18]. All tests are performed at a constant room temperature, approximately 21 °C, using the standardized pendulum Charpy impact test machine PW 15 by Otto Wolpert GmbH, with a maximum impact energy of 147.1 Joules. For the 0 degrees orientation, two types of Charpy specimens are investigated: with the notch root in only one deposition layer ,i.e. transverse, (T) and with the notch root containing multiple deposition layers, i.e. lateral, (L), as shown in Figure 1. This distinction is made to test the difference in toughness between the orientations parallel (T) and perpendicular (L) to the plane of deposition. The Charpy specimens in both the 45 and 90 degrees have the notch root in one deposition layer (T), which is indicated as 45T and 90T, respectively.

2.3 Rotating bending fatigue tests

To characterize the high-cycle fatigue behaviour of WAAM 308L SS, rotating bending tests are executed. For these tests, cylindrical specimens are used with tangentially blending fillets between the test section and the ends according to ASTM E466-21, as shown in Figure 3. These specimens have a circumferentially machined surface roughness of 1.6 µm.

The rotating bending machine used in this research is the Italsigma RB35, with a maximum bending moment M=35Nm. This machine applies a constant and uniform bending moment over the specimen, which rotates up to 9000 RPM, resulting in a fully reversed stress fluctuation, i.e. a stress ratio R=-1. The stress amplitude equals $\sigma_a = M/W_{el}$, where W_{el} [mm^3] is the elastic section modulus of the test cross-section. Due to the fact that the stress distribution is not uniform over the cross-section, the results of the tests are deemed to be less influenced by the potential presence of internal defects [18]. From these tests, the stress level and the number of cycles can be used to determine the SN-curve according to ASTM E739-10 [19].

3 Results and Discussion

3.1 Monotonic tensile properties

The stress-strain diagrams obtained from the tests are plotted in Figure 4. The dashed lines represent the stress-strain diagrams obtained for the cases where the crosshead displacement has been increased after yielding. On the other hand, the solid lines are obtained for the cases with a constant crosshead speed. It can be observed that the material response to the increased crosshead displacement results in a discontinuity in the stress-strain diagram. Moreover, a different strain hardening behaviour is observed, although it is not consistent between the different directions as it appears to be less pronounced for the 45 degrees orientation. The results obtained from the tensile tests are displayed in Table 2 where all parameters are obtained by the extensometer, except for the Poisson's ratio which is obtained by the DIC measurements.

Contrary to other research performed on WAAM 308L SS [2,7,13], the 0.2% proof stress decreases for all orientations compared to the base material, reported equal to 390 MPa, according to the EN ISO 14343-A:2017 material certificate). Possible explanations could be either a decrease in dislocation density due to annealing as discussed in [2] or an increase in residual stresses due to the exposure to non-uniform heat during production.

Figure 5 shows the agreement between the linear elastic material model used to estimate Young's modulus and the stress-strain diagram. As can be observed, the proportionality limit is significantly lower than the 0.2% proof stress, conventionally indicating yield stress. Moreover, it can be seen that a larger scatter is present for the 0 degrees orientation as compared to the other orientations. This difference in scatter can be explained by the deposition layer orientation of the specimens. Figure 1 shows the different deposition layer orientations for the three specimen orientations. For 0 degrees, the location of the specimen in the WAAM plate is of large significance, as it may affect the number of stacked layers within the test section of the specimen. The Young modulus for WAAM 308L SS differs significantly for each specimen orientation and from the base material E_{base}=200 GPa [20]. Mechanical and microstructural fibering, caused by the WAAM production method, is the most obvious explanation for these differences [7,8,13]. As a consequence, Young's modulus is the highest in the 45 degrees orientation which may be attributed to a high density of grains loaded in the <110> direction [15].

The Poisson's ratio is evaluated for the same elastic range over which the Young's modulus is determined. All three specimens with a 0 degrees orientation show a relatively similar relationship between transverse and axial strain for which an averaged Poisson's ratio of 0.50 can be calculated. The same applies to the 90 degrees orientation, for which a Poisson's ratio of 0.36 can be determined. Comparing both directions shows that the visible scatter is larger for the 90 degrees specimens, while the standard deviation is larger for the 0 degrees direction, $\hat{\sigma}_{\nu_0}$=0.06 and $\hat{\sigma}_{\nu_{90}}$=0.02. To determine the Poisson's ratio for the 45 degrees orientation, special attention should be given to T.45.2. This specimen has a significantly different transverse strain compared to the other two 45 degrees specimens. Nonetheless, the data point cloud shows an approximately similar trend as for specimens T.45.3 and T.45.4. For that reason, it is chosen to release the intercept and determine Poisson's ratio by fitting a linear relationship without an intercept. This results in an average Poisson's ratio of 0.01 in the 45 degrees orientation.

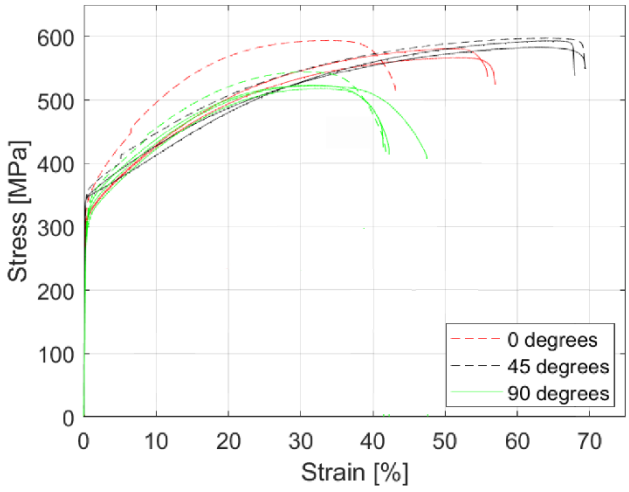

Figure 4 Stress-strain diagrams resulting from the monotonic tensile tests

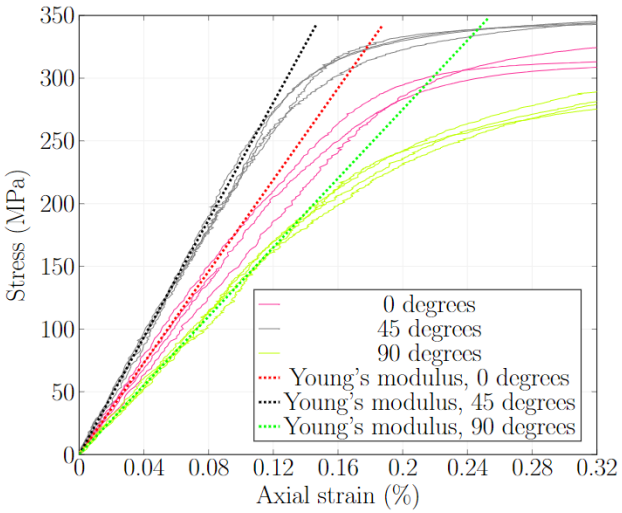

Figure 5 Stress-strain diagrams in the elastic region and linear elastic model

Figure 6 shows that the axial strain field is different per orientation, indicating an anisotropic behaviour. The axial strain field of the 45 degrees direction shows a clear 45 degrees angle, which exposes the deposition layer. For the 0 and 90 degrees orientation, the deposition layers are less visible. The strain fields show local strains scattered over the tested section, from which no clear orientation can be distinguished.

Besides the exposure of the 45 degrees orientation, Figure 6 also shows that at a force of 34 kN, the axial strain in the 45 degrees specimen is significantly higher over a larger

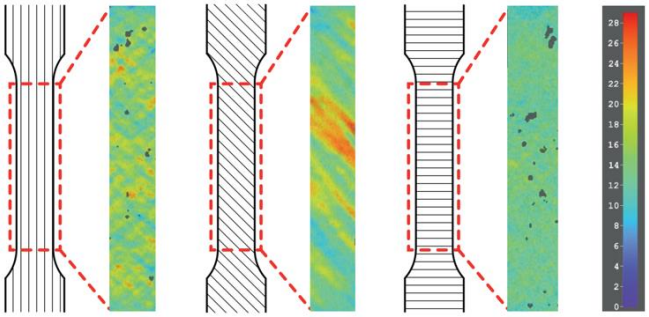

Figure 6 Axial strain field per orientation at an applied force of 34kN, i.e. 544MPa.

area compared to the other two orientations. Besides, the 90 degrees orientation shows a significantly lower axial strain compared to the other two orientations, which is in line with the stress-strain diagrams in Figure 4.

As can be deduced from Table 2, the specimens extracted in the 45 degrees orientation have the highest parameters regarding ductility. Overall, most parameters are the highest for the 45 degrees orientation. However, the reduction of area - which indicates necking in tensile tests - is lowest for the 45 degrees orientation. The same can be seen when comparing the maximum strain to the strain at ultimate tensile stress: for the 45 degrees orientation, these are close to each other. The 90 degrees orientation is the least ductile when considering the maximum strain, the strain at the ultimate tensile stress and the modulus of toughness. The reduction of area is however the highest, indicating significant necking.

The ductility parameters obtained from the stress-strain diagrams, Figure 4, also indicate strain-rate sensitivity for the 0 degrees orientation as the modulus of toughness is 21.3% lower compared to the specimens tested at a lower crosshead speed. For the other specimen orientations, there is no significant difference in ductility parameters due to a difference in strain rate.

Table 2 Results of the monotonic tensile tests indicating mean (upper value) and standard deviation (lower value)

		Orientation		
		0	**45**	**90**
Young's Modulus	[GPa]	182.47 16.82	233.80 7.67	137.55 5.44
Poisson's ratio	[-]	0.50 0.06	0.01 0.01	0.36 0.02
Yield stress	[MPa]	316.08 7.73	346.21 2.53	297.56 7.60
Ultimate tensile stress	[MPa]	577.06 7.61	590.17 5.66	526.89 10.14
Strain at fracture	[%]	54.04 6.41	66.82 2.74	43.36 2.45
Strain at UTS	[%]	47.91 8.48	66.29 2.42	43.36 2.45
Reduction of area	[%]	56 3	50 5	65 2
Modulus of toughness	[GPa]	24.49 2.77	35.99 0.84	20.45 1.15

3.2 Charpy impact toughness tests

The results from the standardized Charpy impact toughness tests are displayed in Figure 7. The specimens having an orientation of 45 and 90 degrees exhibited an impact energy higher than the machine limit. Furthermore, a significant difference can be found between the T and L directions within the 0 degrees orientation, where the T orientation has a lower impact energy. This means that the impact energy absorption is higher when loaded parallel to the deposition layers compared to perpendicular to the layers.

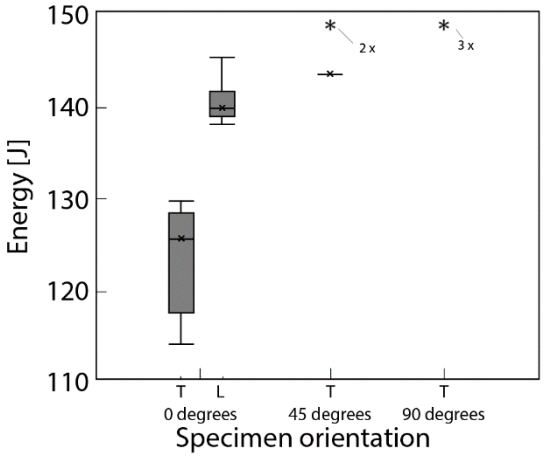

Figure 7 Results of the Charpy impact toughness tests, symbol * indicates an impact toughness higher than the limit of the testing machines.

3.3 Fatigue tests

The first fatigue test was executed at a rotational speed of 7000 rpm, corresponding to a loading frequency of 116.7 Hz. Nonetheless, during this test self-heating of the specimen has been observed, see Figures 8 and 9.

The self-heating phenomenon is attributed to a combination of the loading frequency and the stress distribution over the cross-section. For static conditions, the material is able to find a thermal equilibrium with the surroundings. Nonetheless, in the case of fast cyclic loading, the material does not have sufficient time to find thermal equilibrium with the environment. The same applies to unloading. As a consequence, the stress-strain diagram would show a hysteresis loop rather than a linear relationship. This results in energy that cannot be dissipated by the specimen, which means that heat generates and self-heating of the specimen occurs [8]. In addition, stainless steel is more prone to self-heating due to its reduced thermal conductivity as compared to carbon steel. This phenomenon is also caused by the shape of the test specimen, having a uniform cross-section.

To determine the fatigue properties without temperature influences, a sufficiently low loading frequency is used. This is done by subsequently doing tests at lower frequencies. Eventually, at a rotational speed of 2500 RPM, i.e. 41.7 Hz, limited self-heating could be observed. For that reason, it is chosen to execute the subsequent fatigue tests at this rotational speed.

Figure 8 shows the test results in the S-N plot. The test results are divided depending on the loading frequency, clearly showing the effect of self-heating on the fatigue life. Moreover, the specimens which did not fail have been retested at a significantly higher stress amplitude. However, special attention should be given to the possible occurrence of the coaxing effect [21].

The S-N curve for the 90 degrees orientation is visualized in Figure 8, based on the green data points excluding the overheated specimens. The SN-curve shows a relatively narrow range of stress amplitudes, i.e. 280-290 MPa, corresponding to a high-cycle fatigue regime.

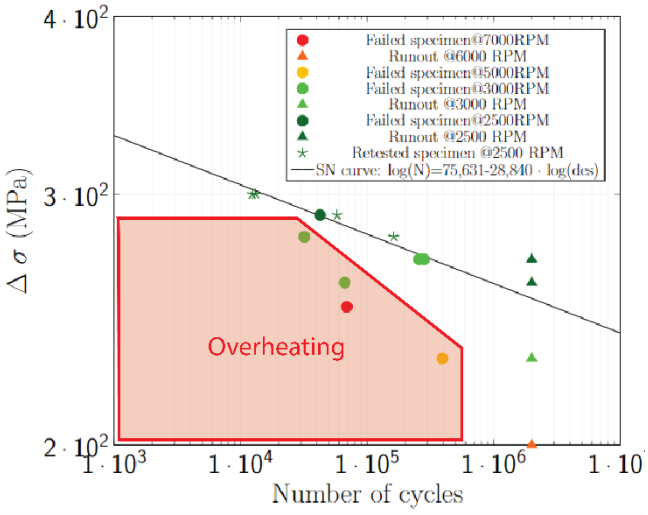

Figure 8 Test results and S-N curve for the 90 degrees orientation

Figure 9 Fracture surface of a self-heated specimen

4 Conclusions

In this research, the fatigue behaviour and monotonic tensile properties of WAAM 308L stainless steel are investigated.

The monotonic tensile properties of WAAM 308L SS differ significantly depending on the orientation of loading. The 45 degrees orientation has the highest yield stress, ultimate stress, Young's modulus and elongation (which applies to both the maximum strain and the strain at the ultimate tensile stress), whilst the 90 degrees orientation has the highest reduction of area and the 0 degrees orientation the highest Poisson's ratio.

The yield strength of WAAM 308L SS is decreased for all orientations compared to the base material 308L SS. This may be caused by a decrease in dislocation density as suggested in previous literature or an increase in residual stresses originating from non-uniform heating during fabrication.

Regarding the toughness, no clear conclusions can be drawn. Only the notch in the longitudinal direction is tougher compared to the transverse direction regarding the 0 degrees of orientation.

WAAM 308L SS is strain rate sensitive. Increasing the crosshead speed during tensile tests showed an increase in stress without a strain difference, indicating strain rate sensitivity.

WAAM 308L SS is prone to self-heating under a high strain rate at cyclic loading. Rotating bending tests at relatively high rotation speed resulted in specimens significantly heating up and showing a significantly lower fatigue life. This self-heating phenomenon was not observed during tests at lower rotational speeds, which indicates the susceptibility to self-heating under high strain rates.

Acknowledgement

The authors would like to acknowledge Jean-François Moulin and MX3D for manufacturing the 308L SS WAAM plates. This paper is the result of a project which is part of the Boost! Project "The strength of additive manufactured metals against fatigue".

References

[1] Duan, X., Li, Q., Xie, W., & Yang, X. (2023). Wire arc metal additive manufacturing using pulsed arc plasma (PAP-WAAM) for effective heat management. *Journal of Materials Processing Technology*, *311*, 117806.

[2] Li, Y., Yuan, Y., Wang, D., Fu, S., Song, D., Vedani, M., & Chen, X. (2022). Low cycle fatigue behavior of wire arc additive manufactured and solution annealed 308 L stainless steel. *Additive Manufacturing*, *52*, 102688.

[3] Shamsaei, N., Yadollahi, A., Bian, L., & Thompson, S. M. (2015). An overview of Direct Laser Deposition for additive manufacturing; Part II: Mechanical behavior, process parameter optimization and control. *Additive Manufacturing*, *8*, 12-35.

[4] Shamsaei, N., & Fatemi, A. (2014). Small fatigue crack growth under multiaxial stresses. *International Journal of Fatigue*, *58*, 126-135.

[5] Cunningham, C. R., Dhokia, V., Shokrani, A., & Newman, S. T. (2021). Effects of in-process LN2 cooling on the microstructure and mechanical properties of type 316L stainless steel produced by wire arc directed energy deposition. *Materials Letters*, *282*, 128707.

[6] Yehorov, Y., da Silva, L. J., & Scotti, A. (2019). Exploring the use of switchback for mitigating homoepitaxial unidirectional grain growth and porosity in WAAM of aluminium alloys. *The International Journal of Advanced Manufacturing Technology*, *104*, 1581-1592.

[7] Laghi, V., Palermo, M., Tonelli, L., Gasparini, G., Ceschini, L., & Trombetti, T. (2020). Tensile properties and microstructural features of 304L austenitic stainless steel produced by wire-and-arc additive manufacturing. *The International Journal of Advanced Manufacturing Technology*, *106*, 3693-3705.

[8] Dieter, G. E., Metallurgy, J. M., & Edition, S. M. (1988). McGraw-Hill Book Company.

[9] Mouritz, A. P. (2012). *Introduction to aerospace materials*. Elsevier.

[10] Li, M., Lu, T., Dai, J., Jia, X., Gu, X., & Dai, T. (2020). Microstructure and mechanical properties of 308L stainless steel fabricated by laminar plasma additive manufacturing. *Materials Science and Engineering: A*, *770*, 138523.

[11] Laghi, V., Tonelli, L., Palermo, M., Bruggi, M., Sola, R., Ceschini, L., & Trombetti, T. (2021). Experimentally-validated orthotropic elastic model for wire-and-arc additively manufactured stainless steel. *Additive Manufacturing*, *42*, 101999.

[12] Hadjipantelis, N., Weber, B., Buchanan, C., & Gardner, L. (2022). Description of anisotropic material response of wire and arc additively manufactured thin-walled stainless steel elements. *Thin-Walled Structures*, *171*, 108634.

[13] Kyvelou, P., Slack, H., Mountanou, D. D., Wadee, M. A., Britton, T. B., Buchanan, C., & Gardner, L. (2020). Mechanical and microstructural testing of wire and arc additively manufactured sheet material. *Materials & Design*, *192*, 108675.

[14] van Nuland, T. F., Van Dommelen, J. A. W., & Geers, M. G. (2021). Microstructural modeling of anisotropic plasticity in large scale additively manufactured 316L stainless steel. *Mechanics of Materials*, *153*, 103664.

[15] Bayerlein, U., & Sockel, H. G. (1992). Determination of single crystal elastic constants from DS-and DR-Ni-based superalloys by a new regression method between 20C and 1200C. *Superalloys*, 695-704.

[16] ASTM E8M-21. Standard practice for conducting force-controlled constant amplitude axial fatigue tests of metallic materials. *American Society for Testing and Materials International*.

[17] ASTM E23-02. Standard test methods for notched bar impact testing of metallic materials. *American Society for Testing and Materials International*.

[18] Morel, F., Morel, A., & Nadot, Y. (2009). Comparison between defects and micro-notches in multiaxial fatigue–The size effect and the gradient effect. *International journal of fatigue*, *31*(2), 263-275.

[19] ASTM E739-10. Standard Practice for Statistical Analysis of Linear or Linearized Stress-Life (S-N) and Strain-Life (ε-N) Fatigue Data1. *American Society for Testing and Materials International*.

[20] ASMIH Committee. ASM Handbook, Volume 01-Properties and Selection: Irons, Steels, and High-Performance Alloys. *ASM International*.

[21] Ishihara, S., & McEvily, A. J. (1999). A coaxing effect in the small fatigue crack growth regime. *Scripta Materialia*, *40*(5), 617-622.